ACS Photonics

pubs.acs.org/journal/apchd5

Article

Probing Charge Generation Efficiency in Thin-Film Solar Cells by Integral-Mode Transient Charge Extraction

Stefan Zeiske, Oskar J. Sandberg,* Jona Kurpiers, Safa Shoaee, Paul Meredith, and Ardalan Armin*

Cite This: *ACS Photonics* 2022, 9, 1188−1195

Read Online

ACCESS | Metrics & More | Article Recommendations

ABSTRACT: The photogeneration of free charges in light-harvesting devices is a multistep process, which can be challenging to probe due to the complexity of contributing energetic states and the competitive character of different driving mechanisms. In this contribution, we advance a technique, integral-mode transient charge extraction (ITCE), to probe these processes in thin-film solar cells. ITCE combines capacitance measurements with the integral-mode time-of-flight method in the low intensity regime of sandwich-type thin-film devices and allows for the sensitive determination of photogenerated charge-carrier densities. We verify the theoretical framework of our method by drift-diffusion simulations and demonstrate the applicability of ITCE to organic and perovskite semiconductor-based thin-film solar cells. Furthermore, we examine the field dependence of charge generation efficiency and find our ITCE results to be in excellent agreement with those obtained via time-delayed collection field measurements conducted on the same devices.

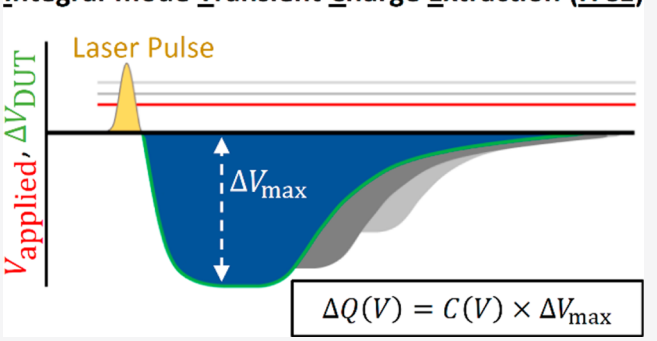

KEYWORDS: *charge generation, thin-film solar cells, organic semiconductors, perovskite semiconductors, external generation efficiency*

Organic semiconductors are characterized by incomplete free charge carrier generation at room temperature, which is directly related to their excitonic nature by a virtue of their low permittivity and thus incomplete screening of the electron−hole Coulomb force. To improve the charge generation efficiency, bulk heterojunctions (BHJ) comprising electron-donating (donor, D) and -accepting (acceptor, A) organic semiconductors are employed as the photoactive material in so-called BHJ organic solar cells (OSC). Free charge generation in these semiconductors ordinarily involves multiple steps starting with the photogeneration of singlet excitons in either the D or the A domains, followed by exciton diffusion to the D/A interface. At the D/A interface, excitons can undergo charge transfer (i.e., electron transfer from D to A or hole transfer from A to D) and form interfacial charge-transfer (CT) states,[1,2] comprising Coulombically bound donor cations and acceptor anions. The charge transfer process (sometimes referred to as charge generation) is believed to be independent of any applied external electric field and predominantly energetically and kinetically driven.[3] This mechanism can create photovoltage as the chemical potential of CT states becomes nonzero after charge generation,[4] but it does not necessarily result in a considerable photocurrent. Efficient generation of free charge carriers (essential for photocurrent) requires CT states to quickly dissociate to free charges before decaying back to the ground state.[5−7]

However, the mechanism of CT state dissociation into free charges is still a matter of debate despite intensive studies over several decades. While the work of Braun[8] implied that CT dissociation in OSCs is field-dependent, most efficient D/A blends show either no or only weak dependence on the electric field.[9−12] Hence, more advanced models have been proposed to explain the fast and efficient dissociation of CT states to free charges. Clarke and Durrant, for instance, considered the role of entropy in CT dissociation events,[6] while other models include the role of energetic disorder,[13] delocalization,[14,15] and vibronically excited (i.e., "hot") states[16] in the formation of free, separated charges. The role of "hot CT states" was challenged by Kurpiers and co-workers, who found the electric field and temperature dependent charge generation in fullerene acceptor (FA)-based BHJs to be independent of excess energy.[12] They concluded, in line with past findings by Vandewal et al.,[2] that charge generation proceeds through thermalized CT states, independent of activation energies and the energetic offset between relaxed singlet exciton and CT

Received: October 8, 2021
Published: March 31, 2022

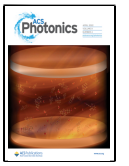

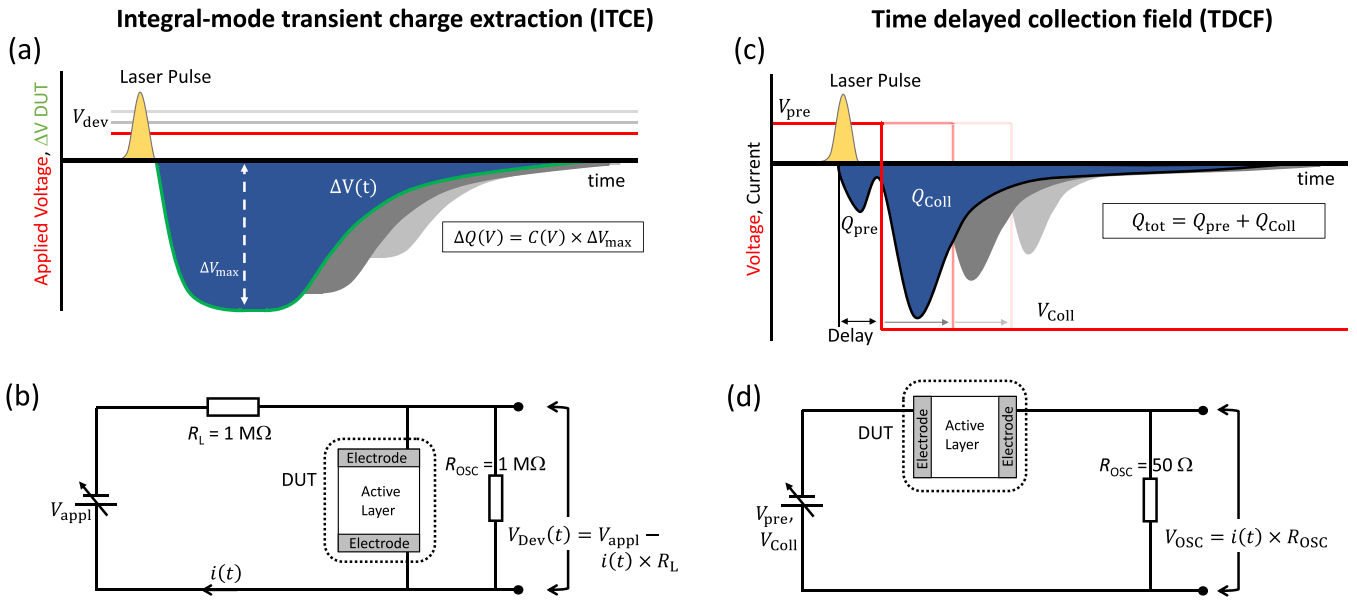

Figure 1. (a) Schematic timeline of an integral-mode transient charge extraction (ITCE) experiment. While the bias V_{dev} is applied on the DUT, a short laser pulse at $t = 0$ photogenerates charge carriers in the DUT active layer. The photoinduced change in voltage drop acorss the DUT active layer is measured by an oscilloscope in parallel with the DUT. The green (red) solid line indicates the corresponding photovoltage transient (applied device bias V_{dev}). (b) Circuit of an ITCE experiment. A large load resistance R_L is in series with the DUT, while the change in photoinduced voltage drop across the DUT is measured by an oscilloscope with large input resistance configured in parallel. (c) Schematic timeline of a time delayed collection field (TDCF) experiment. At the time $t = 0$ a short laser pulse photogenerates charge carriers in the acitve layer of the DUT, while it is held under a prebias V_{pre}. After a short delay time, a high reverse collection bias V_{coll} is applied on the DUT to extract all photogenerated charge carriers. The red (black) solid line indicates the correpsonding applied voltage (photocurrent) transient. (d) Simplified circuit of a TDCF experiment, where the DUT is in series with an oscilloscope with R_{OSC} = 50 Ω input impedance.

states. This is also to be expected in the new class of state-of-the-art OSCs based on nonfullerene acceptors (NFA) exhibiting low energetic offsets. Despite this, recent studies on CT dissociation conducted on NFA systems suggested an electric field and excess energy dependent charge generation.[17] Furthermore, Karuthedath and co-workers proposed a model based on interfacial D/A band-bending inducing quadrupole moments, suggesting the requirement for an ionization energy offset to drive charge generation in both FA- and NFA-based OSCs.[18,19]

To gain more insight into the process of CT state dissociation, methods capable of probing free charge generation efficiency in thin-film solar cells independent of bulk recombination are needed. This has proven to be challenging but, if successful, could guide a better understanding of the mechanism of charge generation in state-of-the-art OSCs and thus aid molecular and architecture improvements. In the past, several measurement techniques have been employed to investigate free charge generation in optoelectronic devices. While intensity dependent photocurrent (IPC)[20] and external (internal) quantum efficiency [EQE (IQE)][21−23] are prominent examples of steady-state techniques, transient absorption spectroscopy (TAS)[24−26] and time-delayed collection field (TDCF) are, in turn, commonly used time-resolved techniques. Probing charge generation using IPC is questionable, as the results can be affected by first-order losses due to trap-assisted recombination and the so-called pseudo-first-order recombination near the electrodes.[27,28] TAS, in turn, has been used to probe free charge generation via detecting geminate recombination at early time scales.[20,29] However, TAS measurements are often performed in the transmission mode on thin films and not on fully optimized solar cell devices containing reflective back-electrodes. TDCF has been the most useful method and is frequently used to study the free charge generation dynamics in organic and perovskite solar cells.[12,30,31] However, while TDCF remains a powerful methodology, it uses a complex circuit requiring specialist current preamplifiers with fast bias ramp-up times and suffers from *RC*-time limitations at short time scales.

In this work we advance an alternative and potentially more straightforward measurement technique to probe charge generation in optoelectronic devices. The technique is based on an extension of the integral-mode time-of-flight method[32] in the low-intensity regime, which accounts for capacitive effects associated with the sandwich-type thin-film device structure. In contrast to TDCF, the proposed method does not suffer from limitations induced by *RC* effects, allows for a sensitive measurement of charge carrier density at very low pulse fluence without a reduced signal accuracy, and does not require ultrasensitive fast preamplifiers. The new method, however, has a more limited voltage range than TDCF. The analytical framework behind the technique, integral-mode transient charge extraction (ITCE), is derived and verified by drift-diffusion (DD) simulations. Finally, to demonstrate the method, we apply the technique to thin-film organic semiconductor and perovskite semiconductor (as a second verifying system) solar cells and probe the field-dependent external generation efficiency (EGE), finding good agreement of experimental results obtained via ITCE and TDCF conducted on the same devices.

METHODS AND MATERIALS

All devices were fabricated on ITO-patterned glass substrates (Lumtec). After cleaning the ITO substrates in DI water, acetone, and isopropanol, substrates were first dried by a

https://doi.org/10.1021/acsphotonics.1c01532
ACS Photonics 2022, 9, 1188−1195

nitrogen flow and then treated with a plasma for 1 min. Subsequently, 30 nm layers of PEDOT:PSS (Clevios PVP AI 4083) were spin-coated on substrates at 6000 rpm for 40 s, followed by thermal annealing under an inert atmosphere at 150 °C for 15 min. For PCDTBT:$PC_{70}BM$ active layers, PCDTBT (M_n = 65−85 kDa; purchased from Solaris Chem. Inc.54) and $PC_{70}BM$ (phenyl-C71-butyric acid methyl ester; purchased from Solenne BV) were mixed in dichlorobenzene at a concentration of 35 mg/mL with a donor/acceptor ratio of 1:4 (wt) and spin-coated at 2000 rpm to form a 100 nm thick film. For the neat PCDTBT active layer, 20 mg/mL PCDTBT was dissolved in chlorobenzene and spin-coated at 2000 rpm to form a 100 nm thick film. Triple cation perovskite active layers with a thickness of approximately 300 nm were prepared according to ref 33 using 10 nm PTAA as a hole-transport layer and 30 nm C_{60} and 7 nm LiF as an electron-transport layer. PCDTBT:$PC_{70}BM$ and neat PCDTBT (perovskite) devices were finalized by evaporating 7 nm Ca and 100 nm Al (8 nm BCP and 100 nm copper) through a shadow mask defining a pixel area of 0.16 cm^2. Afterward, all devices were sealed with a cover glass using UV light-annealed glue (Bluefix).

A Newport Oriel Sol2A simulator in combination with a Keithley 2400 source-measure unit was used for current density versus applied voltage (J−V) characterization. A KG3 filtered reference silicon cell (calibrated at the Fraunhofer ISE) was used to calibrate the solar simulator to the standard AM 1.5G condition (100 mW cm^{-2}).

The schematic and circuit diagram of our ITCE method are shown in Figure 1a,b. Similar to the integral-mode time-of-flight method,[32] a large load resistor and an external voltage source (to provide an external voltage V_{appl} to the circuit) are connected in series with the device under test (DUT). However, to record the voltage across the device, an oscilloscope is configured in parallel to the DUT. A short laser pulse is used to generate charge carriers in the bulk of the DUT. A diode-pumped, Q-switched Nd:YAG laser (Quantel, Viron Version A) operating a 532 nm excitation wavelength, 6.84 ns pulse width, 0.04 μJ cm^{-2} pulse fluence, and 20 Hz repetition rate is used in combination with a Standa 10MVAA attenuator to generate charge carriers in the bulk of the DUT. A Keithley 2450 is used to apply voltages across the DUT, which is in series with a 1 MΩ load resistor. The voltage transients are recorded with an oscilloscope (Rohde and Schwarz, RTM 3004) with 1 MΩ input resistance in parallel with the DUT. For dark C−V measurements, an E5061B ENA Network Analyzer with modulation frequency of 1 kHz and a bandwidth of 10 Hz is used. The voltage drop across the DUT is measured by a Keithley 2450.

Figure 1c,d schematically shows a simplified circuit and triggering diagrams of a typical TDCF experimental setup. Here, a variable prebias V_{pre} is applied on the operational photovoltaic DUT using an external voltage source, while a short laser photopulse leads to the generation of charge carriers in the photoactive layer. After a certain delay time t_{delay}, the photogenerated charges are extracted by applying a collection bias V_{coll} (typically a high reverse bias). An oscilloscope is used to record the current flowing through the DUT, and by integrating the extraction photocurrent transient, the total number of extracted charge carriers can be obtained. More details of the TDCF setup are provided elsewhere.[34]

THEORY

ITCE is based on connecting the sandwich-type thin-film diode or solar cell device in series with a large load resistance R_L and a voltage source applying a DC bias V_{appl}. The device is initially kept under DC conditions, with the corresponding voltage drop across the device being given by $V_{dev} = V_{appl} - i_0R_L$, where i_0 is the DC current through the circuit. At the time $t = 0$, a light pulse is applied to the device, resulting in charge carriers being generated inside the active layer. The photogenerated electrons and holes are subsequently transported under the influence of the internal electric field toward the cathode and anode, respectively, giving rise to a transient current $i(t)$ and a voltage drop $V(t) = V_{appl} - i(t)R_L$ across the device.

In general, with the anode assumed to be located at $x = 0$ and the cathode at $x = d$ (d is the active layer thickness), the corresponding time-dependent current density $j(t) = i(t)/A$ (where A is the device area) is independent of the position x in the device and given by[35]

$$j(t) = j_c(x, t) + \varepsilon\varepsilon_0\frac{\partial E(x, t)}{\partial t} \tag{1}$$

Here, $E(x,t)$ is the electric field and $j_c(x,t)$ is the conduction current density given by the sum of the individual electron and hole current densities, which both on the other hand depend on the position x in the active layer and the time t; ε is the relative permittivity and ε_0 is the permittivity of the vacuum. Furthermore, the photoinduced change in the voltage drop $\Delta V(t) = V(t) - V_{dev}$ is related to the change of the electric field within the active layer via

$$\frac{\partial \Delta V(t)}{\partial t} = \int_0^d \frac{\partial E(x, t)}{\partial t}\,\mathrm{d}x \tag{2}$$

Subsequently, upon taking the spatial average over the active layer of the total current in eq 1 and making use of eq 2, we obtain

$$\frac{\Delta V(t)}{R_L} + C_{geo}\frac{\partial \Delta V(t)}{\partial t} = -\Delta i_c(t) \tag{3}$$

where $\Delta i_c(t) = (A/d)\int_0^d j_c(x,t)\,\mathrm{d}x - i_0$ is the change in the spatially averaged conduction currents induced by the light pulse (note that $\Delta i_c(t) = 0$ for $t < 0$), while $C_{geo} = \frac{\varepsilon\varepsilon_0 A}{d}$ is the geometrical capacitance of the active layer.

For large load resistances ($R_LC_{geo} \to \infty$), eq 3 simplifies to $\partial\Delta V(t)/\partial t = -\Delta i_c(t)/C_{geo}$. Under these conditions, the maximal induced change in the voltage is given as $\Delta V_{max} = \Delta Q/C_{geo}$, where $\Delta Q = -\int_0^{t_{extr}}\Delta i_c(t)\,\mathrm{d}t$ is the total charge induced by the light pulse, while t_{extr} is the time taken for all photogenerated charge carriers to be extracted at the electrodes. After accounting for nonuniform charge distributions, it can be shown that ΔQ is related to the charge carrier densities inside the active layer via[36−38]

$$\Delta Q = \frac{qA}{d}\int_0^d [x\Delta p(x) + (d - x)\Delta n(x)]\,\mathrm{d}x \tag{4}$$

assuming negligible charge carrier recombination (i.e., low intensity condition) and no trapping during the extraction process ($0 < t \le t_{extr}$). Here, $\Delta p(x) = p(x,0) - p(x,t_{extr})$ and $\Delta n(x) = n(x,0) - n(x,t_{extr})$, where $p(x,t)$ [$n(x,t)$] is the hole [electron] density within the active layer at position x and time t.

https://doi.org/10.1021/acsphotonics.1c01532
ACS Photonics 2022, 9, 1188−1195

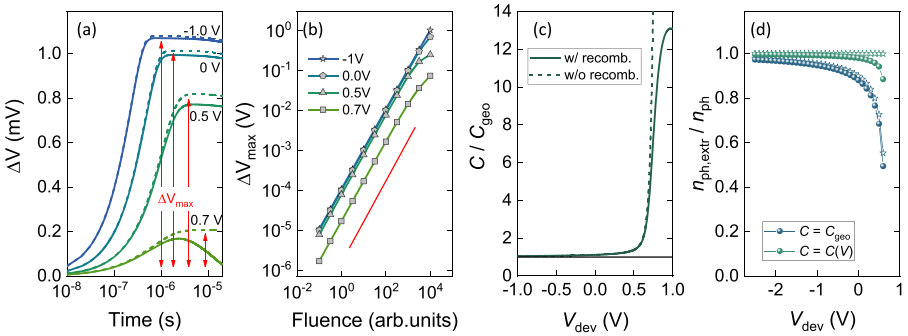

Figure 2. (a) Simulated voltage transients for different applied device voltages V_{dev} and compared for the cases with (solid lines) and without (dashed lines) recombination of charge carriers. (b) Voltage transient maxima, ΔV_{max}, as obtained from the simulated voltage transients, plotted as a function of laser pulse fluence. The red solid line is a guide to the eye with a slope of 1. (c) Simulated device capacitance plotted as a function of applied voltage. The capacitance is normalized to the geometrical device capacitance C_{geo} (horizontal black line). The case with (without) recombination is indicated by solid (dashed) lines. (d) The extracted charge carrier density ($n_{ph,extr}$), normalized to the generated carrier density (n_{ph}), as obtained from the simulated voltage transients, and plotted as a function of device voltage V_{dev}. Sphere-shaped (star-shaped) symbols correspond to the case with (without) recombination of charge carriers.

In general, $\Delta p(x)$ and $\Delta n(x)$ can be expressed as $\Delta p(x) = n_{ph}(x) + \Delta p_0(x)$ and $\Delta n(x) = n_{ph}(x) + \Delta n_0(x)$, where $n_{ph}(x)$ is the initial photogenerated carrier density at $t = 0$ and $\Delta p_0(x)$ [$\Delta n_0(x)$] is the related induced change in the dark background hole [electron] density inside the active layer. In the case of an undoped device with noninjecting contacts, the background densities are negligibly small, and the active layer may be treated as an insulator; for this simplified case, eq 4 reduces to $\Delta Q = C_{geo}\Delta V_{max} = q\overline{n}_{ph}Ad$, where $\overline{n}_{ph} \equiv (1/d)\int_0^d n_{ph}(x)\,dx$ is the spatial average of the photogenerated carrier density at $t = 0$. However, most OSCs employ ohmic contacts. In these devices there exists a nonzero dark background density of electrons and holes, diffused from the contacts, accumulating near the cathode and anode contact, respectively.[38] These dark charge distributions near the contacts effectively reduce the thickness of the insulator-like region in the active layer, resulting in an increased device capacitance relative to C_{geo}.

Accounting for the presence of dark charge carriers, eq 4 can be expressed as $\Delta Q = q\overline{n}_{ph}Ad - \Delta Q_0$. Here, $\Delta Q_0 = -\frac{qA}{d}\int_0^d [x\Delta p_0(x) + (d-x)\Delta n_0(x)]\,dx$ represents the corresponding charge induced by the difference between the background charge density profiles between $t = 0$ and $t = t_{extr}$. However, since the background charge carrier profiles are determined by the prevailing applied voltage and electric field distribution (in contrast to the photogenerated charge $q\overline{n}_{ph}Ad$), ΔQ_0 is capacitive, associated with a redistribution of the background charge profiles induced by the voltage change ΔV_{max} across the device. For small voltage perturbations ΔV_{max}, we thus expect $\Delta Q_0 = (\partial Q_0/\partial V)\Delta V_{max}$. Provided that $t_{extr} \ll R_L C$ (large R_L), we then finally obtain

$$\overline{n}_{ph} = \frac{C}{qAd}\Delta V_{max} \tag{5}$$

where

$$C = C_{geo} + \frac{\partial Q_0}{\partial V} \tag{6}$$

is the voltage-dependent steady-state capacitance of the device in the dark at $V = V_{dev}$. Hence, by measuring ΔV_{max} via ITCE as a function of the voltage V_{dev} across the device, in conjunction with dark device capacitance C, allows for $\overline{n}_{ph}$ versus V_{dev} to be calculated.

To verify the analytical treatment, we applied it to the result obtained from time-dependent DD simulations. The details of the DD model have been provided elsewhere.[38] Briefly, in the simulations, we assumed a trap-free and undoped active layer with a thickness of 100 nm, a dielectric constant $\varepsilon = 3$, balanced mobilities of 10^{-4} cm^2 V^{-1} s^{-1} for electrons and holes, and a bimolecular recombination coefficient of $\beta = 5 \times 10^{-12}$ cm^3 s^{-1}, corresponding to a Langevin reduction factor of ~24. Further, a built-in voltage (V_{bi}) of 1.2 V and ohmic contacts that are perfectly selective for the extraction of electrons and holes at the cathode and anode contact, respectively, were assumed. The device was specified to have an electrical area of $A = 0.04$ cm^2 and connected in series with a large load resistance of $R_L = 1$ MΩ. The corresponding geometric capacitance of the device is $C_{geo} \approx 1.1$ nF, amounting to an RC time of roughly 1 ms. Finally, the photogenerated carriers (introduced at $t = 0$) were taken to be generated with a uniform rate inside the active layer, with the corresponding density $\overline{n}_{ph} = n_{ph}$ assumed to be directly proportional to the pulse fluence. In this regard, geminate (first-order) recombination losses of excitons and charge-transfer states are assumed to be effectively included in n_{ph}. To better demonstrate the capacitive effect, n_{ph} was assumed to be independent of the electric field in the simulations.

Figure 2a shows the simulated voltage transients (solid lines) for different V_{dev} ranging between −1 V and 0.7 V. The corresponding ΔV_{max} are plotted as a function of pulse fluence for different V_{dev} in Figure 2b. In Figure 2c, on the other hand, the device capacitance C under steady-state conditions in the dark (corresponding to low frequencies) is simulated as a function of V_{dev}. In general, it can be seen that ΔV_{max} follows a linear dependence with the fluence at small ΔV_{max}. At large enough fluences, however, ΔV_{max} eventually deviates from linearity as both higher order recombination and screening of the prevailing electric field start to play a role (as ΔV_{max} becomes comparable to V_{dev}). On the other hand, ΔV_{max} is seen to strongly depend on V_{dev} at low fluences. We note that this dependence is present even for the idealized case when no recombination of charge carriers is present ($\beta = 0$, dashed lines). Instead, the V_{dev} dependence of ΔV_{max} is a consequence of the associated induced redistribution of the dark background charge carrier profile inside the active layer. As V_{dev} is increased, the diffusion of injected dark charges (from the

https://doi.org/10.1021/acsphotonics.1c01532
ACS Photonics 2022, 9, 1188−1195

electrodes) penetrates deeper into the bulk, effectively reducing the thickness of the neutral (insulator-like) region inside the active layer, manifest as an increased device capacitance relative to the geometrical capacitance C_{geo} (cf. eq 6). Figure 2d shows the extracted charge carrier density $n_{ph,extr}$, as obtained from the simulations using eq 5, relative to the input photogenerated carrier density n_{ph}. Indeed, $n_{ph,extr}$ is closely given by n_{ph} when the device capacitance $C(V)$ (Figure 2c) is used in eq 5. In contrast, if $C = C_{geo}$ is assumed instead, a deviation between $n_{ph,extr}$ and n_{ph} is observed, resulting in an underestimation of the photogenerated carrier density by a factor of C/C_{geo}. In devices with ohmic contacts (Figure 2c), this underestimation becomes strongly dependent on the voltage in the forward bias and may be mistaken as an apparent field dependence of EGE; hence, to correctly obtain n_{ph}, the voltage dependence of the device capacitance must be accounted for.

We note that there is a small deviation taking place between $n_{ph,extr}/n_{ph}$ of the cases with and without recombination in the active layer at large V_{dev} approaching the built-in voltage; this deviation can be attributed to additional (pseudo)first-order recombination taking place between photogenerated charge carriers and dark background charge carriers near the electrodes.[27,39] In principle, this additional loss may be minimized by tuning the optical electric field (e.g., careful choice of the laser wavelength or the introduction of optical spacer layer) such that the generation profile peaks in the middle of the active layer and is minimal near the electrodes. It should be stressed that, in the case of nonideal contacts, surface recombination (i.e., the collection of minority carriers at the "wrong" electrode) may become prevalent as well, presenting an additional voltage-dependent first-order recombination channel.[40]

From the above presented theoretical and numerical analyses, we conclude that photogenerated charge carrier densities in thin-film solar cells can be measured sensitively via ITCE, when (i) higher-order recombination processes are not present, and (ii) (voltage dependent) carrier back-injection and diffusion-mediated redistribution of dark background charges in the photoactive layer of the DUT are accounted for. While (i) can be addressed by recording ITCE voltage transients at low pulse fluence and avoiding too high ΔV_{max} (ΔV_{max} should be as small as possible, preferably well below 10 mV), (ii) can be addressed by accurately measuring the voltage-dependent device capacitance (at low enough frequencies) in the dark. In the following, we will implement those findings and probe the EGE in different thin-film organic semiconductor and perovskite semiconductor solar cells.

RESULTS AND DISCUSSION

We first applied ITCE to the well-understood model organic solar cell, PCDTBT:$PC_{70}BM$, to further validate the theoretical/numerical findings. Furthermore, we examined neat PCDTBT photovoltaic cells, as well as a high efficiency triple cation perovskite thin-film solar cells. We studied the field dependent EGE in these systems via ITCE and compared these data with benchmark TDCF results. To this end, EGE is evaluated as a function of V_{dev}, noting that the (DC) electric field is expected to be uniform and scale linearly as $E = (V_{dev} - V_{bi})/d$, with V_{bi} on the order of 1 V in these devices. This is expected to be a good approximation for thin active layers and voltages well below V_{bi}.

Figure 3a shows the dark capacitances of all three devices plotted as a function of device voltage, V_{dev}. As shown, the

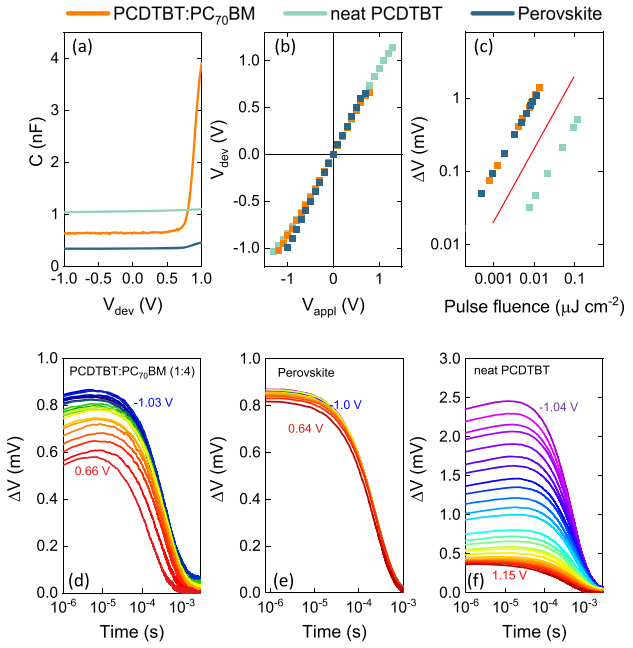

Figure 3. (a) Device capacitance in the dark plotted as a function of voltage and compared with PCDTBT:$PC_{70}BM$ (1:4), neat PCDTBT, and perovskite thin-film solar cells. A bandwidth of 10 Hz and modulation frequencies of 1 kHz (PCDTBT:$PC_{70}BM$ (1:4), neat PCDTBT) and 50 kHz (perovskite) were used. (b) Relation between applied circuit voltages (V_{appl}) and the measured voltage drops (V_{dev}) across the three devices. (c) Maximum change ΔV_{max}, as obtained from voltage transients, for all three solar cells plotted as a function of laser pulse fluence. The excitation wavelength was set to λ_{exc} = 532 nm, and no bias voltage was applied on the devices (short-circuit). The red solid line is a guide to the eye with a slope of 1, indicating the absence of higher-order photocurrent loss mechanisms. (d) Voltage transients of a PCDTBT:$PC_{70}BM$ (1:4) thin-film solar cell compared for different applied bias voltages. (e) Repetition of panel (d), but plotted for a perovskite solar cell. (f) Repetition of panel (d), but plotted for a neat PCDTBT solar cell.

PCDTBT:$PC_{70}BM$ and perovskite thin film solar cells show changes in device capacitance when V_{dev} approaches V_{bi}. To account for the DC voltage loss across the load resistance, the relations between the applied circuit voltage V_{appl} and the measured voltage drop V_{dev} across the PCDTBT:$PC_{70}BM$, neat PCDTBT, and perovskite thin-film devices are depicted in Figure 3b. On the other hand, Figure 3c shows the ΔV_{max} at short-circuit, as obtained from the voltage transients, plotted as a function of laser pulse fluence, and compared for all three thin-film solar cells. We took great care to avoid high laser pulse fluences (which induce substantial bimolecular recombination) when recording the voltage transients at different V_{dev}. The red solid line in Figure 3c is a guide to the eye with a slope of 1, indicating the absence of higher-order (e.g., bimolecular) recombination processes. The corresponding ITCE voltage transients for the PCDTBT:$PC_{70}BM$, neat PCDTBT, and perovskite solar cell are shown in Figure 3d–f, from which ΔV_{max} was obtained at the voltage plateaus.

From the $C-V$ curves and voltage transients we calculated the EGE, which was determined based on the photogenerated charge carrier density (n_{ph}) and the pulse photon density (N_{ph})

https://doi.org/10.1021/acsphotonics.1c01532
ACS Photonics 2022, 9, 1188–1195

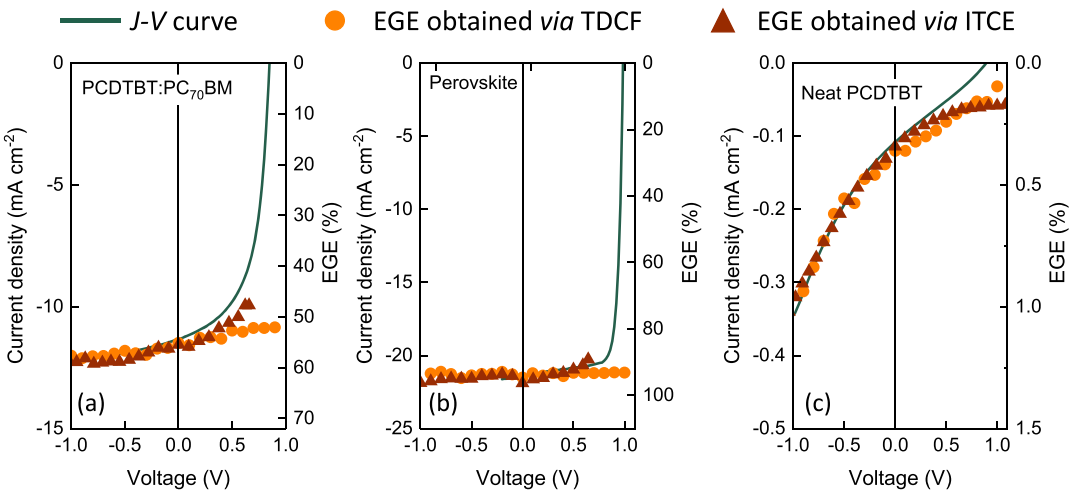

Figure 4. (a) $J-V$ characteristics (solid line) of a thin-film PCDTBT:$PC_{70}BM$ (1:4) solar cell measured under artificial 1 sun (AM 1.5G) illumination and compared with the external generation efficiency (EGE) obtained via TDCF (orange symbols) and ITCE (red symbols). (b) Repetition of panel (a), but plotted for a thin-film perovskite solar cell. (c) Repetition of panel (a), but plotted for a neat PCDTBT device.

via EGE = n_{ph}/N_{ph}, where $N_{ph} = \frac{\lambda F}{hcAd}$, λ is the laser pulse excitation wavelength, h is the Planck constant, and F denotes the pulse fluence (in the unit of J). The ITCE results were cross-calibrated with those obtained via TDCF conducted on the same devices. Figure 4a compares the $J-V$ curve of the PCDTBT:$PC_{70}BM$ solar cell (solid line) with the EGE obtained via ITCE (red symbols) and TDCF (orange symbols). Our ITCE-based EGE results are in excellent agreement with those obtained via TDCF. We find the EGE in PCDTBT:$PC_{70}BM$ to show a weak field dependence decreasing slightly with increasing forward bias voltages. We note, however, that due to expected nonuniform electric fields and uncertainties in the measured device capacitance at high voltages (i.e., when V_{dev} approaches the built-in voltage), the trustable EGE regime in ITCE is limited to V_{dev} below ~0.66 V in the forward bias direction. This is partly due to the rapid increase of the capacitance with voltage (see Figure 3a), where the value of C becomes more sensitive to small voltage fluctuations (ΔV_{max}) and partly due to strong recombination and space charge effects affecting the measured capacitance at large bias.

In a similar manner, we investigated the EGE in a thin-film perovskite solar cell (see Figure 4b), where we find the EGE to be field-independent. Again, our ITCE results (red symbols) show good agreement with those obtained via TDCF. Similar to the PCDTBT:$PC_{70}BM$ device, the trustable V_{dev} window is, when probed by ITCE, limited to ~0.64 V in forward bias direction. We note that perovskites are quite different to organic semiconductors in that they are predominantly nonexcitonic at room temperature and thus demonstrate a more general (if not universal) applicability of ITCE to thin-film photovoltaic devices.

Finally, we investigated a system with an electric field-dependent EGE. To this end, a neat PCDTBT thin-film device was used. It is well-established that single-component organic solar cells exhibit field dependent charge generation.[41,42] Therefore, a neat PCDTBT device is an appropriate model system to observe the field dependence. We note that the capacitance of this device showed a weaker voltage dependence (see Figure 3a), allowing for the capacitance to be accurately measured over the entire voltage range. Subsequently, as shown in Figure 4c, the field-dependent EGE results obtained via ITCE (red symbols) and TDCF (orange symbols) are in excellent agreement over the entire bias voltage regime.

In contrast to the PCDTBT:$PC_{70}BM$ and perovskite devices, the accuracy of the neat PCDTBT $C-V$ measurement at large forward bias voltages was not influenced by carrier diffusion and back-injection from the electrodes into the photoactive layer; this can mainly be attributed to the nonohmic injection character of one or both of the electrodes, suppressing strong recombination and space charge effects at large voltages. In this regard, it should be noted that the EGE is a property of the photoactive layer, hence a modification of the device stack aimed at a more precise $C-V$ measurement (or, suppression of diffusion of injected dark charges, recombination, and the buildup of space charge) allows for accurate ITCE measurements over the entire voltage regime.

CONCLUSIONS

We have presented a transient measurement technique, ITCE, to probe charge generation efficiency in thin-film solar cells, which is based on the sensitive measurement of pulsed, photoinduced changes in voltage drop across the active layer, combined with capacitance measurements. A simple series-circuit with large RC-time is used to generate voltage transients at low laser pulse fluence from which the maximum change in active layer voltage drop can be determined. We derived and verified the theoretical framework of ITCE by DD simulations and demonstrated its applicability by probing the field dependence of EGE in thin-film perovskite and organic solar cells. Our results are in good agreement with those obtained via TDCF conducted on the same devices.

Despite the limitations of ITCE at high forward bias voltages due to uncertainties in the accurate measurement of the device capacitance, ITCE operates at very low pulse fluence (avoiding higher-order recombination) and does not suffer from RC-time limitations. Hence, ITCE with its much simpler circuit allows the measurement of small charge carrier densities sensitively and can be used in a complementary manner with the more complex TDCF method to probe the field dependence of charge generation in thin film solar cells.

https://doi.org/10.1021/acsphotonics.1c01532
ACS Photonics 2022, 9, 1188−1195

AUTHOR INFORMATION

Corresponding Authors

Oskar J. Sandberg − *Sustainable Advanced Materials (Sêr-SAM), Department of Physics, Swansea University, Swansea SA2 8PP Wales, United Kingdom;* orcid.org/0000-0003-3778-8746; Email: o.j.sandberg@swansea.ac.uk

Ardalan Armin − *Sustainable Advanced Materials (Sêr-SAM), Department of Physics, Swansea University, Swansea SA2 8PP Wales, United Kingdom;* orcid.org/0000-0002-6129-5354; Email: ardalan.armin@swansea.ac.uk

Authors

Stefan Zeiske − *Sustainable Advanced Materials (Sêr-SAM), Department of Physics, Swansea University, Swansea SA2 8PP Wales, United Kingdom*

Jona Kurpiers − *Disordered Semiconductor Optoelectronics, Institute of Physics and Astronomy, University Potsdam, 14476 Potsdam-Golm, Germany*

Safa Shoaee − *Disordered Semiconductor Optoelectronics, Institute of Physics and Astronomy, University Potsdam, 14476 Potsdam-Golm, Germany;* orcid.org/0000-0001-5754-834X

Paul Meredith − *Sustainable Advanced Materials (Sêr-SAM), Department of Physics, Swansea University, Swansea SA2 8PP Wales, United Kingdom*

Complete contact information is available at: https://pubs.acs.org/10.1021/acsphotonics.1c01532

Notes

The authors declare no competing financial interest.

ACKNOWLEDGMENTS

This work was supported by the Sêr Cymru Program through the European Regional Development Fund, Welsh European Funding Office and Swansea University strategic initiative in Sustainable Advanced Materials. A.A. is a Sêr Cymru II Rising Star Fellow and P.M. a Sêr Cymru II National Research Chair. S.S. and J.K. are grateful to the Alexander von Humboldt foundation for their support. This work was funded by UKRI through the EPSRC Program Grant EP/T028511/1 Application Targeted Integrated Photovoltaics.

REFERENCES

(1) Vandewal, K. Interfacial charge transfer states in condensed phase systems. *Annu. Rev. Phys. Chem.* **2016**, *67*, 113−133.

(2) Vandewal, K.; et al. Efficient charge generation by relaxed charge-transfer states at organic interfaces. *Nat. Mater.* **2014**, *13*, 63−68.

(3) Armin, A.; Li, W.; Sandberg, O. J.; Xiao, Z.; Ding, L.; Nelson, J.; Neher, D.; Vandewal, K.; Shoaee, S.; Wang, T.; Ade, H.; Heumuller, T.; Brabec, C.; Meredith, P. A history and perspective of non-fullerene electron acceptors for organic solar cells. *Adv. Energy Mater.* **2021**, *11*, 2003570.

(4) Sandberg, O. J.; Armin, A. Energetics and kinetics requirements for organic solar cells to break the 20% power conversion efficiency barrier. *J. Phys. Chem. C* **2021**, *125*, 15590.

(5) Laquai, F.; Andrienko, D.; Deibel, C.; Neher, D. Charge carrier generation, recombination, and extraction in polymer-fullerene bulk heterojunction organic solar cells. *Adv. Polym. Sci.* **2017**, *272*, 267−291.

(6) Clarke, T. M.; Durrant, J. R. Charge photogeneration in organic solar cells. *Chem. Rev.* **2010**, *110*, 6736−6767.

(7) Proctor, C. M.; Kuik, M.; Nguyen, T. Q. Charge carrier recombination in organic solar cells. *Prog. Polym. Sci.* **2013**, *38*, 1941−1960.

(8) Braun, C. L. Electric field assisted dissociation of charge transfer states as a mechanism of photocarrier production. *J. Chem. Phys.* **1984**, *80*, 4157−4161.

(9) Kniepert, J.; et al. Effect of solvent additive on generation, recombination, and extraction in PTB7:PCBM solar cells: A conclusive experimental and numerical simulation study. *J. Phys. Chem. C* **2015**, *119*, 8310−8320.

(10) Albrecht, S.; et al. On the field dependence of free charge carrier generation and recombination in blends of PCPDTBT/PC 70BM: Influence of solvent additives. *J. Phys. Chem. Lett.* **2012**, *3*, 640−645.

(11) Kniepert, J.; Schubert, M.; Blakesley, J. C.; Neher, D. Photogeneration and recombination in P3HT/PCBM solar cells probed by time-delayed collection field experiments. *J. Phys. Chem. Lett.* **2011**, *2*, 700−705.

(12) Kurpiers, J.; et al. Probing the pathways of free charge generation in organic bulk heterojunction solar cells. *Nat. Commun.* **2018**, *9*, 2038.

(13) Hinrichsen, T. F.; Chan, C. C. S.; Ma, C.; Palecek, D.; Gillett, A.; Chen, S.; Zou, X.; Zhang, G.; Yip, H.-L.; Wong, K. S.; Friend, R. H.; Yan, H.; Rao, A.; Chow, P. C. Y. Long-lived and disorder-free charge transfer states enable endothermic charge separation in efficient non-fullerene organic solar cells. *Nat. Commun.* **2020**, *11*, 5617.

(14) Boguslavskiy, A. E.; et al. The multielectron ionization dynamics underlying attosecond strong-field spectroscopies. *Science (80-.).* **2012**, *335*, 1336−1340.

(15) Bernardo, B.; et al. Delocalization and dielectric screening of charge transfer states in organic photovoltaic cells. *Nat. Commun.* **2014**, *5*, 3245.

(16) Jailaubekov, A. E.; et al. Hot charge-transfer excitons set the time limit for charge separation at donor/acceptor interfaces in organic photovoltaics. *Nat. Mater.* **2013**, *12*, 66−73.

(17) Saladina, M.; et al. Charge Photogeneration in Non-Fullerene Organic Solar Cells: Influence of Excess Energy and Electrostatic Interactions. *Adv. Funct. Mater.* **2021**, *31*, 2007479.

(18) Karuthedath, S.; et al. Intrinsic efficiency limits in low-bandgap non-fullerene acceptor organic solar cells. *Nat. Mater.* **2021**, *20*, 378−384.

(19) Khan, J. I.; Alamoudi, M. A.; Chaturvedi, N.; Ashraf, R. S.; Nabi, M. N.; Markina, A.; Liu, W.; Dela Pena, T. A.; Zhang, W.; Aleveque, O.; Harrison, G. T.; Alsufyani, W.; Levillain, E.; De Wolf, S.; Andrienko, D.; McCulloch, I.; Laquai, F.; et al. Impact of Acceptor Quadrupole Moment on Charge Generation and Recombination in Blends of IDT-Based Non-Fullerene Acceptors with PCE10 as Donor Polymer. *Adv. Energy Mater.* **2021**, *11*, 2100839.

(20) Stolterfoht, M.; et al. Slower carriers limit charge generation in organic semiconductor light-harvesting systems. *Nat. Commun.* **2016**, *7*, 11944.

(21) Armin, A.; et al. Spectral dependence of the internal quantum efficiency of organic solar cells: Effect of charge generation pathways. *J. Am. Chem. Soc.* **2014**, *136*, 11465−11472.

(22) Armin, A.; et al. Quantum efficiency of organic solar cells: Electro-optical cavity considerations. *ACS Photonics* **2014**, *1*, 173−181.

(23) Li, W.; Zeiske, S.; Sandberg, O. J.; Riley, D. B.; Meredith, P.; Armin, A. Organic solar cells with near-unity charge generation yield. *Energy Environ. Sci.* **2021**, *14*, 6484−6493.

(24) Grancini, G.; et al. Hot exciton dissociation in polymer solar cells. *Nat. Mater.* **2013**, *12*, 29−33.

(25) Shoaee, S.; et al. A comparison of charge separation dynamics in organic blend films employing fullerene and perylene diimide electron acceptors. *J. Phys. Chem. Lett.* **2015**, *6*, 201−205.

(26) Zhong, Y.; et al. Sub-picosecond charge-transfer at near-zero driving force in polymer:non-fullerene acceptor blends and bilayers. *Nat. Commun.* **2020**, *11*, 833.

(27) Würfel, U.; et al. Recombination between photogenerated and electrode-induced charges dominates the fill factor losses in optimized organic solar cells. *J. Phys. Chem. Lett.* **2019**, *10*, 3473−3480.
(28) Zeiske, S.; et al. Direct observation of trap-assisted recombination in organic photovoltaic devices. *Nat. Commun.* **2021**, *12*, 3603.
(29) Armin, A.; Durrant, J. R.; Shoaee, S. Interplay between triplet-, singlet-charge transfer states and free charge carriers defining bimolecular recombination rate constant of organic solar cells. *J. Phys. Chem. C* **2017**, *121*, 13969−13976.
(30) Paulke, A.; et al. Charge carrier recombination dynamics in perovskite and polymer solar cells. *Appl. Phys. Lett.* **2016**, *108*, 113505.
(31) Collado-Fregoso, E.; et al. Energy-gap law for photocurrent generation in fullerene-based organic solar cells: The case of low-donor-content blends. *J. Am. Chem. Soc.* **2019**, *141*, 2329−2341.
(32) Österbacka, R.; et al. Quantum efficiency and initial transport of photogenerated charge carriers in π-conjugated polymers. *Synth. Met.* **2003**, *139*, 811−813.
(33) Stolterfoht, M.; et al. The impact of energy alignment and interfacial recombination on the internal and external open-circuit voltage of perovskite solar cells. *Energy Environ. Sci.* **2019**, *12*, 2778−2788.
(34) Kurpiers, J.; Neher, D. Dispersive non-geminate recombination in an amorphous polymer:fullerene blend. *Sci. Rep.* **2016**, *6*, 1−10.
(35) Lampert, M. A.; Mark, P. *Current Injection in Solids*; Academic Press, 1970.
(36) Kniepert, J.; et al. Reliability of charge carrier recombination data determined with charge extraction methods. *J. Appl. Phys.* **2019**, *126*, 205501.
(37) Hawks, S. A.; Finck, B. Y.; Schwartz, B. J. Theory of current transients in planar semiconductor devices: Insights and applications to organic solar cells. *Phys. Rev. Appl.* **2015**, *3*, 044014.
(38) Sandberg, O. J.; Tvingstedt, K.; Meredith, P.; Armin, A. Theoretical perspective on transient photovoltage and charge extraction techniques. *J. Phys. Chem. C* **2019**, *123*, 14261−14271.
(39) Würfel, U.; Unmüssig, M. Apparent field-dependence of the charge carrier generation in organic solar cells as a result of (bimolecular) recombination. *Sol. RRL* **2018**, *2*, 1800229.
(40) Sokel, R.; Hughes, R. C. Numerical analysis of transient photoconductivity in insulators. *J. Appl. Phys.* **1982**, *53*, 7414−7424.
(41) Chamberlain, G. A. Organic solar cells: A review. *Sol. Cells* **1983**, *8*, 47−83.
(42) Deibel, C.; Dyakonov, V. Polymer-fullerene bulk heterojunction solar cells. *Rep. Prog. Phys.* **2010**, *73*, 96401−96439.

https://doi.org/10.1021/acsphotonics.1c01532
ACS Photonics 2022, 9, 1188−1195